DESY 01-100
July 2001

ISSN 0418-9833

arXiv:hep-ex/0108039 23 Aug 2001

# Measurement of $D^{*\pm}$ Meson Production and $F_2^c$ in Deep-Inelastic Scattering at HERA

H1 Collaboration

**Abstract**

The inclusive production of $D^{*\pm}(2010)$ mesons in deep-inelastic scattering is studied with the H1 detector at HERA. In the kinematic region $1 < Q^2 < 100$ GeV$^2$ and $0.05 < y < 0.7$ an $e^+p$ cross section for inclusive $D^{*\pm}$ meson production of $8.50 \pm 0.42$ (stat.)$^{+1.21}_{-1.00}$ (syst.) nb is measured in the visible range $p_{t\,D^*} > 1.5$ GeV and $|\eta_{D^*}| < 1.5$. Single and double differential inclusive $D^{*\pm}$ meson cross sections are compared to perturbative QCD calculations in two different evolution schemes. The charm contribution to the proton structure, $F_2^c\left(x, Q^2\right)$, is determined by extrapolating the visible charm cross section to the full phase space. This contribution is found to rise from about 10% at $Q^2 = 1.5\ \mathrm{GeV}^2$ to more than 25% at $Q^2 = 60\ \mathrm{GeV}^2$ corresponding to $x$ values ranging from $5 \cdot 10^{-5}$ to $3 \cdot 10^{-3}$.

*Submitted to Phys. Lett. B*

C. Adloff[33], V. Andreev[24], B. Andrieu[27], T. Anthonis[4], V. Arkadov[35], A. Astvatsatourov[35], A. Babaev[23], J. Bähr[35], P. Baranov[24], E. Barrelet[28], W. Bartel[10], P. Bate[21], A. Beglarian[34], O. Behnke[13], C. Beier[14], A. Belousov[24], T. Benisch[10], Ch. Berger[1], T. Berndt[14], J.C. Bizot[26], V. Boudry[27], W. Braunschweig[1], V. Brisson[26], H.-B. Bröker[2], D.P. Brown[10], W. Brückner[12], D. Bruncko[16], J. Bürger[10], F.W. Büsser[11], A. Bunyatyan[12,34], A. Burrage[18], G. Buschhorn[25], A.J. Campbell[10], J. Cao[26], T. Carli[25], S. Caron[1], D. Clarke[5], B. Clerbaux[4], C. Collard[4], J.G. Contreras[7,41], Y.R. Coppens[3], J.A. Coughlan[5], M.-C. Cousinou[22], B.E. Cox[21], G. Cozzika[9], J. Cvach[29], J.B. Dainton[18], W.D. Dau[15], K. Daum[33,39], M. Davidsson[20], B. Delcourt[26], N. Delerue[22], R. Demirchyan[34], A. De Roeck[10,43], E.A. De Wolf[4], C. Diaconu[22], J. Dingfelder[13], P. Dixon[19], V. Dodonov[12], J.D. Dowell[3], A. Droutskoi[23], A. Dubak[25], C. Duprel[2], G. Eckerlin[10], D. Eckstein[35], V. Efremenko[23], S. Egli[32], R. Eichler[36], F. Eisele[13], E. Eisenhandler[19], M. Ellerbrock[13], E. Elsen[10], M. Erdmann[10,40,e], W. Erdmann[36], P.J.W. Faulkner[3], L. Favart[4], A. Fedotov[23], R. Felst[10], J. Ferencei[10], S. Ferron[27], M. Fleischer[10], Y.H. Fleming[3], G. Flügge[2], A. Fomenko[24], I. Foresti[37], J. Formánek[30], J.M. Foster[21], G. Franke[10], E. Gabathuler[18], K. Gabathuler[32], J. Garvey[3], J. Gassner[32], J. Gayler[10], R. Gerhards[10], C. Gerlich[13], S. Ghazaryan[4,34], L. Goerlich[6], N. Gogitidze[24], M. Goldberg[28], C. Goodwin[3], C. Grab[36], H. Grässler[2], T. Greenshaw[18], G. Grindhammer[25], T. Hadig[13], D. Haidt[10], L. Hajduk[6], W.J. Haynes[5], B. Heinemann[18], G. Heinzelmann[11], R.C.W. Henderson[17], S. Hengstmann[37], H. Henschel[35], R. Heremans[4], G. Herrera[7,41], I. Herynek[29], M. Hildebrandt[37], M. Hilgers[36], K.H. Hiller[35], J. Hladký[29], P. Höting[2], D. Hoffmann[22], R. Horisberger[32], S. Hurling[10], M. Ibbotson[21], Ç. İşsever[7], M. Jacquet[26], M. Jaffre[26], L. Janauschek[25], D.M. Jansen[12], X. Janssen[4], V. Jemanov[11], L. Jönsson[20], D.P. Johnson[4], M.A.S. Jones[18], H. Jung[20,10], H.K. Kästli[36], D. Kant[19], M. Kapichine[8], M. Karlsson[20], O. Karschnick[11], F. Keil[14], N. Keller[37], J. Kennedy[18], I.R. Kenyon[3], S. Kermiche[22], C. Kiesling[25], P. Kjellberg[20], M. Klein[35], C. Kleinwort[10], T. Kluge[1], G. Knies[10], B. Koblitz[25], S.D. Kolya[21], V. Korbel[10], P. Kostka[35], S.K. Kotelnikov[24], R. Koutouev[12], A. Koutov[8], H. Krehbiel[10], J. Kroseberg[37], K. Krüger[10], A. Küpper[33], T. Kuhr[11], T. Kurča[25,16], R. Lahmann[10], D. Lamb[3], M.P.J. Landon[19], W. Lange[35], T. Laštovička[35], P. Laycock[18], E. Lebailly[26], A. Lebedev[24], B. Leißner[1], R. Lemrani[10], V. Lendermann[7], S. Levonian[10], M. Lindstroem[20], B. List[36], E. Lobodzinska[10,6], B. Lobodzinski[6,10], A. Loginov[23], N. Loktionova[24], V. Lubimov[23], S. Lüders[36], D. Lüke[7,10], L. Lytkin[12], H. Mahlke-Krüger[10], N. Malden[21], E. Malinovski[24], I. Malinovski[24], R. Maraček[25], P. Marage[4], J. Marks[13], R. Marshall[21], H.-U. Martyn[1], J. Martyniak[6], S.J. Maxfield[18], D. Meer[36], A. Mehta[18], K. Meier[14], P. Merkel[10], A.B. Meyer[11], H. Meyer[33], J. Meyer[10], P.-O. Meyer[2], S. Mikocki[6], D. Milstead[18], T. Mkrtchyan[34], R. Mohr[25], S. Mohrdieck[11], M.N. Mondragon[7], F. Moreau[27], A. Morozov[8], J.V. Morris[5], K. Müller[37], P. Murín[16,42], V. Nagovizin[23], B. Naroska[11], J. Naumann[7], Th. Naumann[35], G. Nellen[25], P.R. Newman[3], T.C. Nicholls[5], F. Niebergall[11], C. Niebuhr[10], O. Nix[14], G. Nowak[6], J.E. Olsson[10], D. Ozerov[23], V. Panassik[8], C. Pascaud[26], G.D. Patel[18], M. Peez[22], E. Perez[9], J.P. Phillips[18], D. Pitzl[10], R. Pöschl[26], I. Potachnikova[12], B. Povh[12], K. Rabbertz[1], G. Rädel[27], J. Rauschenberger[11], P. Reimer[29], B. Reisert[25], D. Reyna[10], C. Risler[25], E. Rizvi[3], P. Robmann[37], R. Roosen[4], A. Rostovtsev[23], S. Rusakov[24], K. Rybicki[6], D.P.C. Sankey[5], J. Scheins[1], F.-P. Schilling[13], P. Schleper[10], D. Schmidt[33], D. Schmidt[10], S. Schmitt[10], M. Schneider[22], L. Schoeffel[9], A. Schöning[36], T. Schörner[25], V. Schröder[10], H.-C. Schultz-Coulon[7], C. Schwanenberger[10], K. Sedlák[29], F. Sefkow[37], V. Shekelyan[25], I. Sheviakov[24], L.N. Shtarkov[24], Y. Sirois[27], T. Sloan[17], P. Smirnov[24], V. Solochenko[23,†], Y. Soloviev[24], D. South[21], V. Spaskov[8], A. Specka[27], H. Spitzer[11], R. Stamen[7], B. Stella[31], J. Stiewe[14], U. Straumann[37], M. Swart[14], M. Taševský[29], V. Tchernyshov[23], S. Tchetchelnitski[23], G. Thompson[19], P.D. Thompson[3], N. Tobien[10], D. Traynor[19], P. Truöl[37], G. Tsipolitis[10,38], I. Tsurin[35], J. Turnau[6], J.E. Turney[19], E. Tzamariudaki[25], S. Udluft[25], A. Usik[24], S. Valkár[30], A. Valkárová[30], C. Vallée[22], P. Van Mechelen[4],

S. Vassiliev[8], Y. Vazdik[24], A. Vichnevski[8], K. Wacker[7], R. Wallny[37], B. Waugh[21], G. Weber[11], M. Weber[14], D. Wegener[7], C. Werner[13], M. Werner[13], N. Werner[37], G. White[17], S. Wiesand[33], T. Wilksen[10], M. Winde[35], G.-G. Winter[10], Ch. Wissing[7], M. Wobisch[10], E. Wünsch[10], A.C. Wyatt[21], J. Žáček[30], J. Zálešák[30], Z. Zhang[26], A. Zhokin[23], F. Zomer[26], J. Zsembery[9], and M. zur Nedden[10]

[1] *I. Physikalisches Institut der RWTH, Aachen, Germany*[a]
[2] *III. Physikalisches Institut der RWTH, Aachen, Germany*[a]
[3] *School of Physics and Space Research, University of Birmingham, Birmingham, UK*[b]
[4] *Inter-University Institute for High Energies ULB-VUB, Brussels; Universitaire Instelling Antwerpen, Wilrijk; Belgium*[c]
[5] *Rutherford Appleton Laboratory, Chilton, Didcot, UK*[b]
[6] *Institute for Nuclear Physics, Cracow, Poland*[d]
[7] *Institut für Physik, Universität Dortmund, Dortmund, Germany*[a]
[8] *Joint Institute for Nuclear Research, Dubna, Russia*
[9] *CEA, DSM/DAPNIA, CE-Saclay, Gif-sur-Yvette, France*
[10] *DESY, Hamburg, Germany*
[11] *II. Institut für Experimentalphysik, Universität Hamburg, Hamburg, Germany*[a]
[12] *Max-Planck-Institut für Kernphysik, Heidelberg, Germany*[a]
[13] *Physikalisches Institut, Universität Heidelberg, Heidelberg, Germany*[a]
[14] *Kirchhoff-Institut für Physik, Universität Heidelberg, Heidelberg, Germany*[a]
[15] *Institut für experimentelle und Angewandte Physik, Universität Kiel, Kiel, Germany*[a]
[16] *Institute of Experimental Physics, Slovak Academy of Sciences, Košice, Slovak Republic*[e,f]
[17] *School of Physics and Chemistry, University of Lancaster, Lancaster, UK*[b]
[18] *Department of Physics, University of Liverpool, Liverpool, UK*[b]
[19] *Queen Mary and Westfield College, London, UK*[b]
[20] *Physics Department, University of Lund, Lund, Sweden*[g]
[21] *Physics Department, University of Manchester, Manchester, UK*[b]
[22] *CPPM, CNRS/IN2P3 - Univ Mediterranee, Marseille - France*
[23] *Institute for Theoretical and Experimental Physics, Moscow, Russia*
[24] *Lebedev Physical Institute, Moscow, Russia*[e,h]
[25] *Max-Planck-Institut für Physik, München, Germany*[a]
[26] *LAL, Université de Paris-Sud, IN2P3-CNRS, Orsay, France*
[27] *LPNHE, Ecole Polytechnique, IN2P3-CNRS, Palaiseau, France*
[28] *LPNHE, Universités Paris VI and VII, IN2P3-CNRS, Paris, France*
[29] *Institute of Physics, Academy of Sciences of the Czech Republic, Praha, Czech Republic*[e,i]
[30] *Faculty of Mathematics and Physics, Charles University, Praha, Czech Republic*[e,i]
[31] *Dipartimento di Fisica Università di Roma Tre and INFN Roma 3, Roma, Italy*
[32] *Paul Scherrer Institut, Villigen, Switzerland*
[33] *Fachbereich Physik, Bergische Universität Gesamthochschule Wuppertal, Wuppertal, Germany*[a]
[34] *Yerevan Physics Institute, Yerevan, Armenia*
[35] *DESY, Zeuthen, Germany*[a]
[36] *Institut für Teilchenphysik, ETH, Zürich, Switzerland*[j]
[37] *Physik-Institut der Universität Zürich, Zürich, Switzerland*[j]

[38] *Also at Physics Department, National Technical University, Zografou Campus, GR-15773 Athens, Greece*

[39] *Also at Rechenzentrum, Bergische Universität Gesamthochschule Wuppertal, Germany*
[40] *Also at Institut für Experimentelle Kernphysik, Universität Karlsruhe, Karlsruhe, Germany*
[41] *Also at Dept. Fis. Ap. CINVESTAV, Mérida, Yucatán, México*[k]
[42] *Also at University of P.J. Šafárik, Košice, Slovak Republic*
[43] *Also at CERN, Geneva, Switzerland*

[†] *Deceased*

[a] *Supported by the Bundesministerium für Bildung, Wissenschaft, Forschung und Technologie, FRG, under contract numbers 7AC17P, 7AC47P, 7DO55P, 7HH17I, 7HH27P, 7HD17P, 7HD27P, 7KI17I, 6MP17I and 7WT87P*
[b] *Supported by the UK Particle Physics and Astronomy Research Council, and formerly by the UK Science and Engineering Research Council*
[c] *Supported by FNRS-NFWO, IISN-IIKW*
[d] *Partially Supported by the Polish State Committee for Scientific Research, grant no. 2P0310318 and SPUB/DESY/P03/DZ-1/99, and by the German Federal Ministry of Education and Science, Research and Technology (BMBF)*
[e] *Supported by the Deutsche Forschungsgemeinschaft*
[f] *Supported by VEGA SR grant no. 2/5167/98*
[g] *Supported by the Swedish Natural Science Research Council*
[h] *Supported by Russian Foundation for Basic Research grant no. 96-02-00019*
[i] *Supported by the Ministry of Education of the Czech Republic under the projects INGO-LA116/2000 and LN00A006, and by GA AVČR grant no B1010005*
[j] *Supported by the Swiss National Science Foundation*
[k] *Supported by CONACyT*

# 1 Introduction

Results on inclusive $D^{*\pm}$ meson production in deep-inelastic $ep$ scattering (DIS) and on the charm contribution to the proton structure function, $F_2^c$, at HERA have been published by the H1 and the ZEUS collaborations [1–3]. These data, together with earlier fixed target data [4], have shown clear evidence that the dynamics of charm production in $ep$ scattering is described by the photon gluon fusion process, which is sensitive to the gluon density in the proton [5] and allows its universality to be tested.

Early results on $F_2^c$ from the H1 experiment [1] were based on an integrated luminosity of 3 pb$^{-1}$ collected during the 1994 HERA running and were therefore statistically limited. The current analysis uses data from the 1996 and 1997 HERA running periods, yielding a significantly larger integrated luminosity of 18.6 pb$^{-1}$. Furthermore, the improved instrumentation in the backward region of the H1 detector enables the kinematic range in four-momentum transfer squared to the virtual photon, $Q^2$, to be significantly extended down to $1$ GeV$^2$. Hence, more precise tests of perturbative QCD (pQCD) become possible.

This paper is organized as follows: a short discussion of the different approaches to open charm production in perturbative QCD calculations is followed by a description of the experimental set-up and details of the analysis; the inclusive cross sections for $D^{*\pm}$ meson production are then presented and compared to QCD predictions. Finally, they are used to derive the charm contribution to the proton structure function, $F_2^c$.

# 2 Models of Open Charm Production

The description of open heavy flavour production in electron proton collisions is based on perturbative QCD. In leading order (LO), the photon gluon fusion process ($\gamma g \rightarrow Q\overline{Q}$) is the dominant contribution [1]. Next-to-leading order (NLO) calculations in several schemes are available [6–10]. All approaches assume that $Q^2$ and the heavy quark mass $m_Q$ provide a hard enough scale to allow the applicability of pQCD and to guarantee the validity of the factorization theorem.

Here, the "massive approach" is adopted, i.e. a fixed order calculation with massive quarks assuming three active flavours in the proton. The momentum densities of the three light quarks and the gluon in the proton are evolved by the DGLAP equation [11]. The heavy quarks are assumed to be produced only at the perturbative level [6] via photon gluon fusion. These calculations are considered reliable in the regime $Q^2 \approx m_Q^2$. However, they break down at some scale $Q^2 \gg m_Q^2$ due to large logarithms $\sim \ln(Q^2/m_Q^2)$.

Based on fixed order $\alpha_s^2$ calculations in the coefficient functions [6] programs for different applications were developed. The Riemersma et al. program [7] can be used to calculate inclusive quantities of heavy quark production, like $F_2^c(x, Q^2)$, while the HVQDIS program [8, 12] allows the calculation of exclusive quantities by providing the four-momenta of the outgoing partons. In the version of the program used here charmed quarks are fragmented in the photon - proton centre of mass frame into $D^{*\pm}$ mesons using the Peterson fragmentation function [13], which is controlled by a single parameter $\epsilon_c$. In addition, to account for the experimentally observed $p_t$ smearing of hadrons with respect to the quark direction, the $D^{*\pm}$ meson

has been given a transverse momentum $p_t$ with respect to the charm quark, according to the function $p_t \cdot \exp(-\alpha p_t)$. The parameter $\alpha$ is chosen such that an average transverse momentum $\langle p_t \rangle \approx 350$ MeV is obtained as observed in $e^+e^-$ data [14]. With this procedure it becomes possible to calculate differential inclusive $D^{*\pm}$ meson cross sections in the experimentally visible phase space region.

The CCFM evolution equation [15] is expected to be more appropriate to describe the parton evolution at small $x$. In the parton cascade, gluons are emitted in an angular ordered manner to account for coherence effects. Due to this angular ordering, the gluon distribution depends on the maximum allowed angle in addition to the momentum fraction $x$ and the transverse momentum of the propagator gluon. The cross section is then calculated according to the $k_t$-factorization theorem by convoluting the unintegrated gluon density with the off-shell photon gluon fusion matrix element with massive quarks for the hard scattering process.

It has been shown previously [16] that $F_2$ and $F_2^c$ can be reasonably well described within the CCFM framework. In addition a solution of the CCFM equation has been obtained recently [17] from a fit to $F_2$ which is able to describe the cross section for forward jet production, where significant differences to the expectation in the DGLAP evolution scheme are seen. Using this solution the hadron level Monte Carlo generator CASCADE has been developed [18]. This allows the full generation of charm events including the initial state gluon radiation according to the CCFM equation and the fragmentation of partons by the Lund String model. The fragmentation of charmed quarks to $D^{*\pm}$ mesons is performed using the Peterson fragmentation function.

# 3 Detector and Simulation

The data have been collected with the H1 detector [19] at HERA during the running periods of 1996 and 1997 when HERA operated with 27.5 GeV positrons and 820 GeV protons colliding at a centre of mass energy of $\sqrt{s} = 300$ GeV. The following detector components are important for this analysis. The scattered positron is identified and measured in the SpaCal [20], a lead-scintillating fibre calorimeter situated in the backward region[1] of the H1 detector. The SpaCal also provides time-of-flight information for trigger purposes. A four double-layer backward drift chamber (BDC) [21] is mounted in front of the SpaCal in order to improve the angular measurement of the scattered positron. Charged particle tracks are reconstructed by two cylindrical central jet drift chambers (CJC) [19, 22] placed concentrically around the beam-line in a homogeneous magnetic field of 1.15 Tesla. The CJC also provides trigger information [23] based on the detection of track segments. Double layers of cylindrical multi-wire proportional chambers (MWPC) [24] for triggering purposes are positioned inside and in-between the two jet chambers. The luminosity is determined from the rate of the Bethe-Heitler reaction $ep \to ep\gamma$.

Monte Carlo simulation programs are used to simulate detector effects and to estimate the systematic uncertainties associated with the measurement. For the determination of the acceptance of the detector and the $D^{*\pm}$ selection efficiencies, heavy flavour (charm and bottom) DIS

[1] The positive $z$-axis of the H1 reference frame, which defines the forward direction, is given by the outgoing proton direction.

events are generated using the AROMA 2.2 [25] program. This program, which is based on the DGLAP evolution scheme, simulates neutral current heavy quark production via photon gluon fusion in leading order QCD including parton showers and heavy quark mass effects. The mass of the charm quark is chosen to be $m_c = 1.5$ GeV while the factorization and renormalization scales are set to $\mu = \sqrt{\hat{s}}$, where $\hat{s}$ denotes the square of the invariant mass of the heavy quark system. The GRV94-LO [26] parton density functions (PDF's) are used for the proton. Hadronization is performed in the Lund String Model [27], as implemented in JETSET 7.4 [28]. The momentum fraction of the charm quark carried by the $D^{*\pm}$ meson is determined according to the Peterson model [13] with the fragmentation parameter $\epsilon_c = 0.078$ [29]. The influence of the details of the fragmentation process on the acceptances and efficiencies has been investigated by (a) varying the Peterson fragmentation parameter between $\epsilon_c = 0.035$, as favoured in [30], and $\epsilon_c = 0.1$ which seems to yield a better description of the hadronic final state in $D^{*\pm}$ events, (b) applying the symmetric Lund fragmentation function [27] also to the $D^{*\pm}$ mesons and (c) using the HERWIG [31] program which is based on the cluster hadronization model [32]. The inaccuracy due to the uncertainty in the QCD parameters is studied by varying the charm quark mass $m_c$ and by changing the factorization and renormalization scales to $\mu = \sqrt{Q^2 + 4m_c^2}$. The dependence of the acceptances and efficiencies on the QCD evolution scheme has been determined also by using the CASCADE [17] event generator. Finally, the influence of QED radiation on the efficiency is determined using the RAPGAP [33] program interfaced to HERACLES 4.1 [34]. All Monte Carlo generated events are fed into the GEANT [35] based simulation of the H1 detector and are subjected to the same reconstruction and analysis chain as used for the data.

# 4 Kinematics

This analysis is restricted to those DIS events which have a scattered positron detected in the backward region of the detector. At fixed center of mass energy $\sqrt{s}$ the kinematics of the inclusive scattering process $ep \to eX$ can be completely determined by any two of the independent Lorentz invariant variables: the Bjorken scaling variable $x$, the lepton inelasticity $y$, the four-momentum squared $Q^2 = -q^2$ of the virtual photon and the invariant mass squared $W^2$ of the hadronic final state. In this analysis, these variables are determined from the measurement of the energy $E'_e$ and the polar angle $\Theta_e$ of the scattered positron according to the expressions

$$\begin{aligned} Q^2 &= 4E_e E'_e \cos^2\left(\frac{\Theta_e}{2}\right) & y &= 1 - \frac{E'_e}{E_e}\sin^2\left(\frac{\Theta_e}{2}\right) \\ x &= \frac{Q^2}{ys} & W^2 &= Q^2\left(\frac{1-x}{x}\right) \end{aligned} \tag{1}$$

where $s = 4E_e E_p$ and $E_e$ and $E_p$ denote the energies of the incoming positron and proton, respectively (the positron and proton masses are neglected).

# 5 Event Selection

The events for this analysis were triggered by a coincidence of an electromagnetic cluster in the SpaCal with a charged track signal from the CJC and a vertex which is coarsely reconstructed from the MWPC information. The positron is identified as the most energetic cluster with $E'_e > 8$ GeV as described in [45]. The cluster radius[2] is required to be less than 4 cm, consistent with an electromagnetic energy deposition, and the cluster center of gravity is required to be within 1.5 cm of the extrapolation of a charged track segment from the backward drift chamber BDC. The geometrical acceptance of the SpaCal and BDC imposes a limitation on the positron scattering angle of $\Theta_e < 177.5°$. These limits and requirements restrict the accessible range in $Q^2$ from 1 GeV$^2$ to 100 GeV$^2$ and in the lepton inelasticity to $y < 0.7$. To measure the event kinematic quantities with sufficiently good resolution $y$ is further constrained to $y > 0.05$. Good agreement is observed for all quantities related to the scattered positron between data and the prediction of the AROMA Monte Carlo simulation. The contribution due to photoproduction background, i.e. $Q^2 < 1$ GeV$^2$, is everywhere smaller than 1% in the selected kinematic region.

Charm production is identified by the reconstruction of $D^{*\pm}$ mesons in the decay chain

$$D^{*+} \rightarrow D^0 \pi^+_{slow} \rightarrow (K^- \pi^+)\pi^+_{slow} \; (+c.c.) \tag{2}$$

using the $D^* - D^0$ mass difference method [36]. The decay products are detected in the central track detector. For each accepted track particle identification is applied using the measurement of the energy loss, $\mathrm{d}E/\mathrm{d}x$, in the central track detector. In order to reconstruct a $D^{*\pm}$ meson candidate, unlike-sign charged tracks are first combined to form $K^{\mp}\pi^{\pm}$ pairs in which one of the particles should be consistent with a kaon and the other with a pion according to their $\mathrm{d}E/\mathrm{d}x$ measurements. Among all possible oppositely charged $K^{\mp}\pi^{\pm}$ pairs, those with an invariant mass consistent within $\pm$70 MeV of the $D^0$ mass are combined with a track of a second pion candidate ("$\pi^{\pm}_{slow}$") having a charge opposite in sign to that of the kaon. In Fig. 1 a clear peak is observed in the distribution of the mass difference $\Delta m = m_{K\pi\pi} - m_{K\pi}$ around the nominal $D^{*\pm} - D^0$ mass difference of 145.4 MeV. A fit to this distribution using a Gaussian for the signal and a term $(\Delta m - m_\pi)^\alpha$ for the background yields a total of $973 \pm 40$ $D^{*\pm}$ mesons in the acceptance range of pseudorapidity[3] $|\eta_{K\pi\pi}| < 1.5$ and transverse momentum $p_{t\,K\pi\pi} > 1.5$ GeV.

# 6 Inclusive Cross Sections

The integrated and differential Born level cross sections for $D^{*\pm}$ meson production in DIS are calculated from the observed number $N_{D^{*\pm}}$ of $D^{*\pm}$ candidates, according to

$$\sigma_{\text{vis}}(e^+p \rightarrow e^+ D^{*\pm} X) = \frac{N_{D^{*\pm}}\,(1-r)}{\mathcal{L}_{int} \cdot B \cdot \epsilon \cdot (1+\delta_{rad})}\,. \tag{3}$$

Here, $r$ stands for the contribution of reflections in the $D^0$ mass window, coming from $D^0$ channels other than the one studied in this analysis. The value of $r$ amounts on average to

[2]The cluster radius is defined as $\sum_i \log(E_i) \cdot d_i / \sum_i \log(E_i)$ where the sum runs over all cells in the cluster: $E_i$ is the normalized energy of the cell $i$ and $d_i$ is the distance of the cell $i$ from the cluster centre of gravity.

[3]The pseudorapidity of a particle is defined as $\eta \equiv -\ln\tan(\Theta/2)$.

about 0.03. The integrated luminosity is denoted by $\mathcal{L}_{int}$ while $B$ refers to the branching ratio $B = B(D^{*+} \to D^0\pi^+) \cdot B(D^0 \to K^-\pi^+) = 0.0259 \pm 0.0006$ [37]. The detection efficiency $\epsilon$ is estimated to be 22.5% using AROMA. The radiative correction $\delta_{rad}$ which correct to the single photon exchange cross sections are obtained from the program HECTOR [38]. Depending on the kinematic region $\delta_{rad}$ varies from +0.11 at small $x$ and $Q^2$ to -0.02 at large $Q^2$. For the integrated visible cross section it averages to 0.03.

## 6.1 Integrated Cross Section

The inclusive cross section for $D^{*\pm}$ meson production in the kinematic region $1 < Q^2 < 100\,\mathrm{GeV}^2$ and $0.05 < y < 0.7$, and in the visible $D^{*\pm}$ range $|\eta_{D^*}| < 1.5$ and $p_{t\,D^*} > 1.5$ GeV is found to be

$$\sigma_{vis}(e^+p \to e^+D^{*\pm}X) = 8.50 \pm 0.42(\mathrm{stat.})^{+1.02}_{-0.76}\,(\mathrm{syst.}) \pm 0.65(\mathrm{model})\,\mathrm{nb}.$$

The errors refer to those from statistics, experimental systematics and additional systematics related to the changes in efficiency obtained by using different Monte Carlo generators and varying the model parameters.

The experimental systematic uncertainties are summarized in Table 1. The largest contribution is due to the uncertainty in the track reconstruction efficiency. Other important sources include uncertainties in the extraction of the $D^{*\pm}$ signal, i.e. the determination of the background shape in the $\Delta m$ distribution and the $D^0$ mass resolution. The uncertainties due to model dependencies, as summarized in Table 2, include the incomplete understanding of the fragmentation process, the uncertainty due to the charm quark mass, the sensitivity to the factorization and renormalization scales and the change of acceptance due to QED effects at the positron vertex. The largest effect on the efficiency is observed by changing the charm quark mass from $m_c = 1.5$ GeV in the reference Monte Carlo dataset to $m_c = 1.3$ GeV and by changing the fragmentation models and their parameters.

The visible inclusive $D^{*\pm}$ meson production cross section has been calculated in the NLO DGLAP scheme with the HVQDIS program using the GRV98-HO parton densities in the proton [39]. The predictions range from 5.17 nb for a charm quark mass $m_c = 1.5$ GeV and Peterson fragmentation parameter $\epsilon_c = 0.10$ to 7.02 nb for $m_c = 1.3$ GeV and $\epsilon_c = 0.035$. The hadronization fraction $f(c \to D^{*+}) = 0.233 \pm 0.010 \pm 0.011$ [40] has been used. For the same variation of $m_c$ and $\epsilon_c$, calculations based on the CCFM evolution, as implemented in the CASCADE program, yield a significantly higher cross section of 8.04 nb and 10.77 nb, respectively.

Disregarding the small differences in the kinematic range, good agreement is observed in the inclusive $D^{*\pm}$ meson production cross section with the result obtained by the ZEUS experiment [3]. The measured value of this cross section agrees better with the CASCADE prediction than with that from HVQDIS. In previous publications [1, 5] H1 reported much better agreement between data and predictions from the HVQDIS program. The larger difference obtained now is due to the new determination of the charm quark hadronization fraction $f(c \to D^{*+})$ which is 16% smaller than the previous value.

## 6.2 Differential Cross Sections

In Fig. 2 the inclusive single differential $D^{*\pm}$ cross sections in the visible region are shown as a function of the event variables $W$, $x$ and $Q^2$ and as a function of the $D^{*\pm}$ observables $p_{t\,D^*}$, $\eta_{D^*}$ and the inelasticity $z_{D^*} = P \cdot p_{D^*}/P \cdot q = (E - p_z)_{D^*}/2yE_e$, where $P$, $q$ and $p_{D^*}$ denote the four-momenta of the incoming proton, the exchanged photon and the observed $D^{*\pm}$ meson, respectively. A bin by bin correction to account for QED radiation has been applied.

Fig. 2 also includes the expectations from the HVQDIS program using the GRV98-HO parton density parameterization. The renormalization scale and the factorization scale are set to $\mu = \sqrt{Q^2 + 4m_c^2}$. The charm quark mass and the fragmentation parameter have been varied from $m_c = 1.3$ GeV and $\epsilon_c = 0.035$ to $m_c = 1.5$ GeV and $\epsilon_c = 0.10$. The dark shaded band indicates the uncertainties in the predictions due to these variations. Although the predicted visible cross section is smaller than experimentally observed, the agreement with the data in the shapes of the different single differential cross sections is reasonable. A significant difference is observed in the d$\sigma$/d$\eta$ cross section. For $\eta_{D^*} > 0$ the measured $D^{*\pm}$ meson production cross section is larger than predicted by the calculation. Since in the boson gluon fusion process the forward region ($\eta_{D^*} > 0$) is correlated with small $z_{D^*}$ a similar discrepancy between data and theory is observed at small $z_{D^*}$.

A possible cause of this deviation could be the simplified grafting of fragmentation onto the HVQDIS program. This approach does not account for the colour force between the charm quark and the proton remnant which is expected to result in a drag of the $D^{*\pm}$ meson from the original charm quark direction towards the proton direction. To quantify this 'beam drag effect' [41], a mapping function from the $\eta_c$-$p_{t\,c}$ space to the $\eta_{D^*}$-$p_{t\,D^*}$ space has been constructed using the AROMA Monte Carlo program which includes such effects. This function has then been used instead of the Peterson fragmentation with transverse momentum smearing in the HVQDIS program. No significant change in the $\eta_{D^*}$ and $z_{D^*}$ distributions has been observed by this procedure compared to our original treatment of fragmentation. A better description of the $\eta_{D^*}$ distribution is obtained, however, when using the HERWIG program to extract the mapping function, at the expense of a 10-15% reduction in the visible cross section prediction. It is therefore concluded that the differences between the measurements and the predictions from the HVQDIS program can not be explained by the absence of colour drag effects in these calculations.

Fig. 2 also presents the predictions of the CASCADE program with the same variations of the charm quark mass and the fragmentation parameter. The expectations from the CASCADE program are found to agree better with the data in general and especially in the positive $\eta$ region.

In order to enable the study of correlations among the observables in $D^{*\pm}$ meson production, Figs. 3 and 4 show the double differential inclusive $D^{*\pm}$ cross sections. It is evident that the excess observed in the data with respect to the HVQDIS expectation at large pseudorapidities ($0.5 < \eta_{D^*} < 1.5$) is independent of $Q^2$ and is concentrated at small $p_{t\,D^*}$ and small $z_{D^*}$. It is especially in this phase space region where the CASCADE program better represents the data.

# 7 Charm Contribution to the Proton Structure Function

The charm contribution, $F_2^c(x,Q^2)$, to the proton structure function is obtained by using the expression for the one photon exchange cross section for charm production

$$\frac{d^2\sigma^c}{dxdQ^2} = \frac{2\pi\alpha_{em}^2}{Q^4 x}\left(1+(1-y)^2\right)\ F_2^c(x,Q^2)\ , \tag{4}$$

where the contribution of the longitudinal structure function is neglected. The visible inclusive $D^{*\pm}$ cross sections $\sigma_{\rm vis}^{\rm exp}(x,Q^2)$ in bins of $x$ and $Q^2$ are converted to a bin center corrected $F_2^{c\ \rm exp}(\langle x\rangle,\langle Q^2\rangle)$ by the relation:

$$F_2^{c\ \rm exp}(\langle x\rangle,\langle Q^2\rangle) = \frac{\sigma_{\rm vis}^{\rm exp}(x,Q^2)}{\sigma_{\rm vis}^{\rm theo}(x,Q^2)}\cdot F_2^{c\ \rm theo}(\langle x\rangle,\langle Q^2\rangle)\ , \tag{5}$$

where $\sigma_{\rm vis}^{\rm theo}$ and $F_2^{c\ \rm theo}$ are the theoretical predictions from the model under consideration. The measured values of the visible cross sections, $\sigma_{\rm vis}^{\rm exp}(x,Q^2)$, are listed in Table 3. Following the same line as in previous publications [1, 2, 5] the HVQDIS program by Harris and Smith [12] and the program of Riemersma et al. [6] are used to calculate these quantities in the NLO DGLAP scheme. In the kinematic range of the current analysis the beauty contribution to the proton structure, $F_2^b$, is expected to be of the order of 1 to 2% of $F_2^c$ [42, 43] and is therefore neglected [4].

In Fig. 5a $F_2^c$ is shown as a function of $x$ for different values of $Q^2$ as extracted from the inclusive $D^{*\pm}$ cross sections using $m_c = 1.4$ GeV. The systematic error on the data points includes those described in Sec. 6.2 as well as additional errors coming from the extrapolation in Equation 5. The bands show the predictions based on the gluon density extracted by the H1 NLO DGLAP fit to the inclusive $F_2$ measurement [45]. The width of each band reflects the total uncertainty of the prediction resulting from the uncertainties on this fit, thereby exploiting the full correlations arising from the constraints of the inclusive $F_2$ measurement. The influence of all the individual sources of uncertainties considered in Ref. [45] for the determination of the gluon density and the strong coupling constant $\alpha_s$ has also been investigated here. The most relevant variations with respect to theoretical calculations are the variation of the strong coupling constant $\alpha_s$ in the range $0.113 \le \alpha_s \le 0.167$, of the factorization and renormalization scale $\mu$ in the range $0.5\cdot(Q^2+4m_c^2) \le \mu \le 2\cdot(Q^2+4m_c^2)$ and of the charm quark mass in the range $1.3 \le m_c \le 1.5\,$GeV. The dominant sources of uncertainties are the experimental error on the $F_2$ measurement at very small $x$ and the insufficient knowledge of the charm quark mass in the range of the direct $F_2^c$ measurements. For the displayed bands the different contributions are added in quadrature. Fig. 5a also includes the results of [3] for comparable values of $Q^2$. These measurements suggest a steeper rise at small $Q^2$ towards small $x$ than expected from the calculations based on the gluon density in the proton extracted from the inclusive $F_2$ measurement.

The extraction of $F_2^c$ according to Equation 5 is faced with an intrinsic problem. The measurement covers about 30% of the total phase space for charm production and the estimation

[4] If, however, the beauty cross section turns out to be large [44], its contribution to $D^{*\pm}$ meson production may have to be subtracted from the visible inclusive cross section prior to the determination of $F_2^c$.

of this acceptance fraction depends significantly on the underlying model. To be more explicit, two different calculations may yield the same value for $F_2^{c\ \mathrm{theo}}(\langle x\rangle, \langle Q^2\rangle)$ but may have different acceptances. They may then predict for a bin in $x$ and $Q^2$ different cross sections $\sigma_{\mathrm{vis}}^{\mathrm{theo}}(x, Q^2)$ with consequent different values for $F_2^{c\ \mathrm{exp}}$. To investigate the model dependence $F_2^{c\ \mathrm{exp}}$ is also determined using the CASCADE program with $m_c = 1.4$ GeV and the results are shown in Fig. 5b. The figure includes also the prediction according to the CCFM evolution. Here the bands indicate the uncertainty on this prediction due to the variation of the charm quark mass. The comparison of Figs. 5a and 5b reveals a steeper rise in the predicted charm contribution to the proton structure function at small $x$ in the CCFM evolution than obtained by the NLO DGLAP evolution. Using the acceptances and efficiencies calculated from the CASCADE program the measured values of $F_2^c$ are found to be systematically smaller than those determined with the HVQDIS program. The largest differences (up to $\approx 20\%$) are observed at small $x$ values.

In Fig. 6 $F_2^c$ is shown as a function of $Q^2$ for different values of $x$ using the acceptances as calculated with HVQDIS. As in Fig. 5 the bands indicate the full uncertainty in the DGLAP NLO predictions for a central value of the charm quark mass of $1.4\,\mathrm{GeV}$ using the gluon density extracted from the fit to the inclusive $F_2$ measurement. The full line shows the DGLAP NLO prediction using the gluon density from GRV98-HO. Taking into account the different data sets used for the determinations of the gluon densities, the agreement of the different calculations is reasonable. The data show a steep rise of $F_2^c$ with $Q^2$. The slope, $\partial F_2^c/\partial \ln Q^2$, contributes roughly half of the slope of the inclusive structure function, $\partial F_2/\partial \ln Q^2$, measured at the central $Q^2$ of each $x$ bin in [45] in the range $0.0002 < x < 0.002$. This steep rise is reasonably well reproduced by the NLO DGLAP calculations.

In Fig. 7 the ratio of $F_2^c$ to the inclusive $F_2$ [45] is shown as a function of $x$ for different values of $Q^2$. The contribution of charm production to the total $F_2$ rises from about 10 % at $Q^2$ = 1.5 GeV$^2$ and $x \approx 10^{-4}$ to more than 25 % at $Q^2 \geq 25\,\mathrm{GeV}^2$ and $x \geq 5 \cdot 10^{-4}$. Although this behaviour agrees with expectation, at small $x$ the measured ratio of $F_2^c/F_2$ is larger than predicted in the NLO DGLAP scheme.

# 8 Conclusions

New measurements of differential cross sections for inclusive $D^{*\pm}$ production in deep-inelastic $ep$ scattering are presented. These are compared with predictions based on both NLO DGLAP and CCFM formalisms, the former made using the HVQDIS program [12] and the latter using the CASCADE model [17]. The predictions made using DGLAP formalism tend to undershoot the data, particularly for small $D^*$ transverse momenta, $p_{t\,D^*}$, and positive $D^*$ pseudorapidities, $\eta_{D^*}$. The expectations of the CCFM based model are in better agreement with the data.

Extrapolation of the visible $D^*$ cross section to the full $p_{tD^*}$ and $\eta_{D^*}$ phase space allows extraction of $F_2^c$, the contribution of charm to the proton structure function $F_2$. These extrapolations are seen to depend on the formalism used: that based on the NLO DGLAP formalism typically produces a larger result for $F_2^c$ than that made using the CCFM approach. Both results are presented to allow consistent comparisons using either formalism. The kinematic range presented has been extended to lower $Q^2$ than shown in the previous H1 study, namely

$Q^2 = 1\,\mathrm{GeV}^2$, and thereby to lower $x$. The $F_2^c$ measurements show large scaling violations and a steep rise of $F_2^c$ with decreasing $x$. This rise tends to be steeper than expected from the NLO DGLAP calculations, but agrees well with the CCFM based expectations. Both approaches for the extraction of $F_2^c$ show that the contribution of charm production to $F_2$ exceeds $25\%$ for $Q^2 > 25\,\mathrm{GeV}^2$.

# Acknowledgments

We are grateful to the HERA machine group whose outstanding efforts have made and continue to make this experiment possible. We thank the engineers and technicians for their work in constructing and now maintaining the H1 detector, our funding agencies for financial support, the DESY technical staff for continual assistance and the DESY directorate for the hospitality which they extend to the non DESY members of the collaboration.

# References

[1] C. Adloff *et al.* [H1 Collaboration], Z. Phys. C **72** (1996) 593 [hep-ex/9607012].

[2] J. Breitweg *et al.* [ZEUS Collaboration], Phys. Lett. B **407** (1997) 402 [hep-ex/9706009].

[3] J. Breitweg *et al.* [ZEUS Collaboration], Eur. Phys. J. C **12** (2000) 35 [hep-ex/9908012].

[4] J. J. Aubert *et al.* [European Muon Collaboration], Nucl. Phys. B **213** (1983) 31.

[5] C. Adloff *et al.* [H1 Collaboration], Nucl. Phys. B **545** (1999) 21 [hep-ex/9812023].

[6] E. Laenen, S. Riemersma, J. Smith and W. L. van Neerven, Phys. Lett. B **291** (1992) 325.

[7] E. Laenen, S. Riemersma, J. Smith and W. L. van Neerven, Nucl. Phys. B **392** (1993) 162; E. Laenen, S. Riemersma, J. Smith and W. L. van Neerven, Nucl. Phys. B **392** (1993) 229; S. Riemersma, J. Smith and W. L. van Neerven, Phys. Lett. B **347** (1995) 143 [hep-ph/9411431].

[8] B. W. Harris and J. Smith, Nucl. Phys. B **452** (1995) 109 [hep-ph/9503484]; B. W. Harris and J. Smith, Phys. Lett. B **353** (1995) 535 [Erratum-ibid. B **359** (1995) 423] [hep-ph/9502312].

[9] M. A. Aivazis, J. C. Collins, F. I. Olness and W. Tung, Phys. Rev. D **50** (1994) 3102 [hep-ph/9312319].

[10] J. C. Collins, Phys. Rev. D **58** (1998) 094002 [hep-ph/9806259].

[11] V. N. Gribov and L. N. Lipatov, Yad. Fiz. **15** (1972) 781 [Sov. J. Nucl. Phys. **15** (1972) 438]; V. N. Gribov and L. N. Lipatov, Yad. Fiz. **15** (1972) 1218 [Sov. J. Nucl. Phys. **15** (1972) 675]; L. N. Lipatov, Sov. J. Nucl. Phys. **20** (1975) 94 [Yad. Fiz. **20** (1975) 181]; G. Altarelli and G. Parisi, Nucl. Phys. B **126** (1977) 298; Y. L. Dokshitzer, Sov. Phys. JETP **46** (1977) 641 [Zh. Eksp. Teor. Fiz. **73** (1977) 1216].

[12] B. W. Harris and J. Smith, Phys. Rev. D **57** (1998) 2806 [hep-ph/9706334].

[13] C. Peterson, D. Schlatter, I. Schmitt and P. Zerwas, Phys. Rev. D **27** (1983) 105.

[14] C. Berger *et al.* [PLUTO Collaboration], Z. Phys. C **22** (1984) 103.

[15] M. Ciafaloni, Nucl. Phys. B **296** (1988) 49; S. Catani, F. Fiorani and G. Marchesini, Phys. Lett. B **234** (1990) 339; S. Catani, F. Fiorani and G. Marchesini, Nucl. Phys. B **336** (1990) 18; G. Marchesini, Nucl. Phys. B **445** (1995) 49 [hep-ph/9412327].

[16] J. Kwiecinski, A. D. Martin and P. J. Sutton, Phys. Rev. D **53** (1996) 6094 [hep-ph/9511263]; J. Kwiecinski, A. D. Martin and P. J. Sutton, Z. Phys. C **71** (1996) 585 [hep-ph/9602320].

[17] H. Jung, Nucl. Phys. Proc. Suppl. **79** (1999) 429 [hep-ph/9905554].

[18] H. Jung, "CCFM prediction on forward jets and F2: Parton level predictions and a new hadron level Monte Carlo generator CASCADE," hep-ph/9908497; H. Jung and G. P. Salam, Eur. Phys. J. C **19** (2001) 351 [hep-ph/0012143].

[19] I. Abt *et al.* [H1 Collaboration], Nucl. Instrum. Meth. A **386** (1997) 310 and 348.

[20] R. D. Appuhn *et al.* [H1 SPACAL Group Collaboration], Nucl. Instrum. Meth. A **386** (1997) 397.

[21] H1 Collaboration, Technical proposal for the upgrade of the backward region of the H1 detector, DESY internal report PRC-93/02.

[22] J. Bürger *et al.*, Nucl. Instrum. Meth. A **279** (1989) 217.

[23] T. Wolff *et al.*, Nucl. Instrum. Meth. A **323** (1992) 537.

[24] K. Müller *et al.*, Nucl. Instrum. Meth. A **312** (1992) 457.

[25] G. Ingelman, J. Rathsman and G. A. Schuler, Comput. Phys. Commun. **101** (1997) 135 [hep-ph/9605285].

[26] M. Glück, E. Reya and A. Vogt, Z. Phys. C **67** (1995) 433.

[27] B. Andersson, G. Gustafson and B. Söderberg, Z. Phys. C **20** (1983) 317; M. G. Bowler, Z. Phys. C **11** (1981) 169; D. A. Morris, Nucl. Phys. B **313** (1989) 634.

[28] T. Sjöstrand, Comput. Phys. Commun. **82** (1994) 74.

[29] D. Besson, Eur. Phys. J. C **15** (2000) 218.

[30] P. P. Nason and C. Oleari, Phys. Lett. B **447** (1999) 327 [hep-ph/9811206].

[31] G. Marchesini, B. R. Webber, G. Abbiendi, I. G. Knowles, M. H. Seymour and L. Stanco, Comput. Phys. Commun. **67** (1992) 465.

[32] B. R. Webber, Nucl. Phys. B **238** (1984) 492; G. Marchesini and B. R. Webber, Nucl. Phys. B **310** (1988) 461.

[33] H. Jung, Comput. Phys. Commun. **86** (1995) 147.

[34] A. Kwiatkowski, H. Spiesberger and H. J. Mohring, Comput. Phys. Commun. **69** (1992) 155; A. Kwiatkowski, H. Spiesberger and H. J. Mohring, Z. Phys. C **50** (1991) 165.

[35] R. Brun, F. Bruyant, M. Maire, A. C. McPherson and P. Zanarini, CERN-DD/EE/84-1.

[36] G. J. Feldman *et al.*, Phys. Rev. Lett. **38** (1977) 1313.

[37] D. E. Groom *et al.* [Particle Data Group Collaboration], Eur. Phys. J. C **15** (2000) 1.

[38] A. Arbuzov, D. Bardin, J. Bluemlein, L. Kalinovskaya and T. Riemann, scattering," Comput. Phys. Commun. **94** (1996) 128 [hep-ph/9511434].

[39] M. Glück, E. Reya and A. Vogt, Eur. Phys. J. C **5** (1998) 461 [hep-ph/9806404].

[40] R. Barate *et al.* [ALEPH Collaboration], Eur. Phys. J. C **16** (2000) 597 [hep-ex/9909032].

[41] E. Norrbin, hep-ph/9909437. E. Norrbin and T. Sjöstrand, Eur. Phys. J. C **17** (2000) 137 [hep-ph/0005110].

[42] K. Daum, S. Riemersma, B. W. Harris, E. Laenen and J. Smith, "The heavy flavor contribution to proton structure," hep-ph/9609478.

[43] A. Chuvakin, J. Smith and W. L. van Neerven, Phys. Rev. D **62** (2000) 036004 [hep-ph/0002011].

[44] T. Sloan, "Heavy flavor production at HERA," hep-ex/0105064; H1 Collaboration, "Beauty Production in Deep Inelastic Scattering", Contributed paper and abstract 807 to the International Conference on High Energy Physics, Budapest, Hungary, July 2001, http://www-h1.desy.de/publications/conf/list.EPS2001.html.

[45] C. Adloff *et al.* [H1 Collaboration], Eur. Phys. J. C **21** (2001) 33 [hep-ex/0012053].

| Experimental Systematic Uncertainties | | |
|---|---|---|
| Trigger efficiency | | $\pm$ 0.02 |
| Track detector efficiency | $+0.075$ | $-0.034$ |
| d$E$/d$x$ measurement | | $\pm$ 0.03 |
| $p_t(\pi_{\rm slow})$-cut | | $+0.025$ |
| Background shape | | $\pm$ 0.05 |
| $D^0$ Mass resolution | $+0.04$ | $-0.025$ |
| Reflections | | $\pm$ 0.015 |
| Event kinematics | | $\pm 0.04$ |
| Luminosity measurement | | $\pm$ 0.015 |
| $\gamma p$ contribution | | $<0.004$ |
| Branching ratio | | $\pm$ 0.025 |
| | $+0.12$ | $-0.09$ |

Table 1: Summary of the fractional experimental systematic uncertainties of the inclusive $D^{*\pm}$ meson cross section.

| Model Uncertainties | | |
|---|---|---|
| Fragmentation model | $+0.035$ | $-0.07$ |
| Charm quark mass | $+0.07$ | $-0.02$ |
| Scale $\mu = \sqrt{Q^2 + 4m_c^2}$ | | $-0.015$ |
| QED radiation | | $-0.025$ |
| | | $\pm 0.08$ |

Table 2: Summary of the fractional model dependent uncertainties of the inclusive $D^{*\pm}$ meson cross sections.

| $\log \frac{Q^2}{\text{GeV}^2}$ | $\langle Q^2 \rangle$ [GeV$^2$] | $\log(x)$ | $\langle x \rangle$ [$10^{-3}$] | $\sigma_{vis}$ [nb] | $F_2^c$ (DGLAP) | $F_2^c$ (CCFM) |
|---|---|---|---|---|---|---|
| 0 | 1.5 | -4.8 to -4.2 | 0.05 | $1.11 \pm 0.19\ ^{+0.15}_{-0.28}$ | $0.114 \pm 0.019\ ^{+0.019}_{-0.030}$ | $0.094 \pm 0.016\ ^{+0.014}_{-0.024}$ |
| to 0.375 | | -4.2 to -3.0 | 0.20 | $1.44 \pm 0.28\ ^{+0.55}_{-0.34}$ | $0.053 \pm 0.010\ ^{+0.021}_{-0.013}$ | $0.056 \pm 0.011\ ^{+0.022}_{-0.013}$ |
| 0.375 | 3.5 | -4.6 to -3.6 | 0.13 | $0.95 \pm 0.13\ ^{+0.14}_{-0.13}$ | $0.161 \pm 0.022\ ^{+0.023}_{-0.027}$ | $0.159 \pm 0.021\ ^{+0.024}_{-0.022}$ |
| to 0.625 | | -3.6 to -3.0 | 0.50 | $0.41 \pm 0.07\ ^{+0.11}_{-0.09}$ | $0.082 \pm 0.015\ ^{+0.022}_{-0.018}$ | $0.082 \pm 0.015\ ^{+0.022}_{-0.018}$ |
| 0.625 | 6.5 | -4.0 to -3.6 | 0.20 | $0.72 \pm 0.10\ ^{+0.27}_{-0.08}$ | $0.309 \pm 0.041\ ^{+0.116}_{-0.042}$ | $0.256 \pm 0.034\ ^{+0.097}_{-0.031}$ |
| to 1 | | -3.6 to -3.0 | 0.50 | $1.02 \pm 0.11\ ^{+0.21}_{-0.10}$ | $0.151 \pm 0.017\ ^{+0.032}_{-0.015}$ | $0.153 \pm 0.017\ ^{+0.032}_{-0.015}$ |
| 1 | 12 | -3.6 to -3.0 | 0.50 | $0.59 \pm 0.09\ ^{+0.11}_{-0.11}$ | $0.276 \pm 0.040\ ^{+0.052}_{-0.052}$ | $0.253 \pm 0.037\ ^{+0.048}_{-0.047}$ |
| to 1.25 | | -3.0 to -2.0 | 2.00 | $0.43 \pm 0.07\ ^{+0.16}_{-0.04}$ | $0.174 \pm 0.029\ ^{+0.064}_{-0.018}$ | $0.194 \pm 0.032\ ^{+0.071}_{-0.021}$ |
| 1.25 | 25 | -3.6 to -3.0 | 0.50 | $0.33 \pm 0.06\ ^{+0.08}_{-0.06}$ | $0.508 \pm 0.096\ ^{+0.125}_{-0.087}$ | $0.422 \pm 0.079\ ^{+0.105}_{-0.071}$ |
| to 1.5 | | -3.0 to -2.0 | 2.00 | $0.54 \pm 0.07\ ^{+0.07}_{-0.09}$ | $0.278 \pm 0.037\ ^{+0.035}_{-0.048}$ | $0.273 \pm 0.036\ ^{+0.036}_{-0.047}$ |
| 1.5 | 60 | -3.0 to -2.6 | 2.00 | $0.31 \pm 0.06\ ^{+0.07}_{-0.03}$ | $0.348 \pm 0.066\ ^{+0.077}_{-0.034}$ | $0.362 \pm 0.068\ ^{+0.081}_{-0.035}$ |
| to 2 | | -2.6 to -2.0 | 3.16 | $0.35 \pm 0.06\ ^{+0.09}_{-0.06}$ | $0.272 \pm 0.050\ ^{+0.067}_{-0.044}$ | $0.270 \pm 0.050\ ^{+0.069}_{-0.043}$ |

Table 3: Inclusive $D^{*\pm}$ cross section $\sigma_{vis}$ in bins in $x$ and $Q^2$ for the visible range $|\eta_{D^*}| < 1.5$ and $p_{t\,D^*} > 1.5$ GeV as extracted in the DGLAP scheme. The values given in the columns denoted by $\langle Q^2 \rangle$ and $\langle x \rangle$ are the bin centres at which the values of $F_2^c$ are given. The values of $F_2^c$ extracted in both the DGLAP and CCFM schemes are also presented.

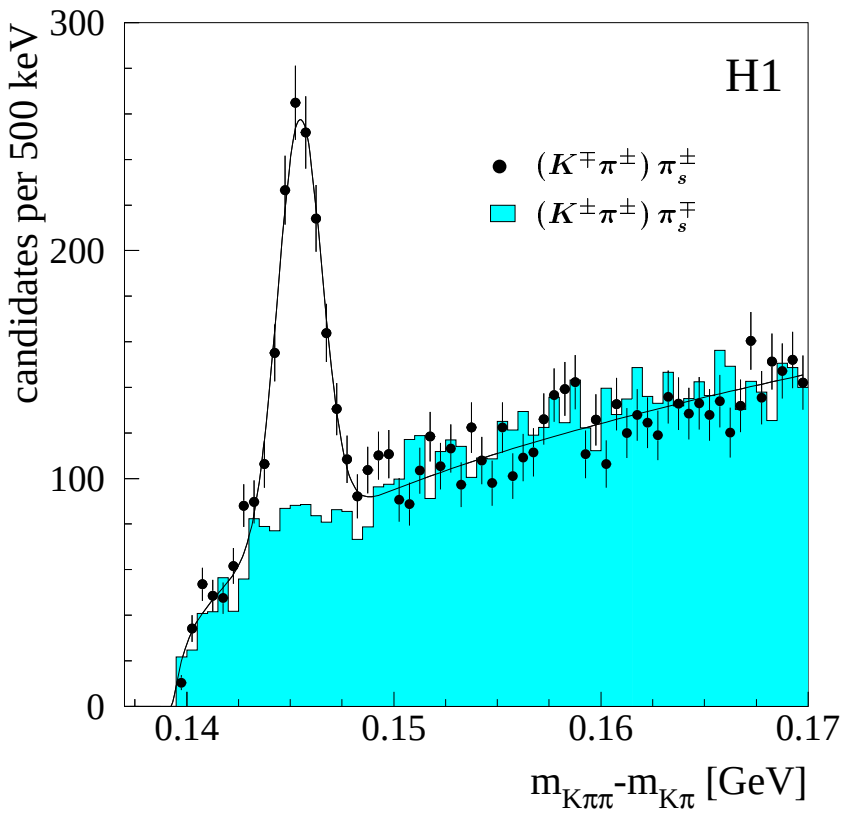


Figure 1: Distribution of the mass difference $\Delta m = m(K^{\mp}\pi^{\pm}\pi_s^{\pm}) - m(K^{\mp}\pi^{\pm})$ for DIS events with $D^0$ candidates in the visible range $|\eta_{K\pi\pi}| < 1.5$ and $p_{t\,K\pi\pi} > 1.5$ GeV. The data points are obtained from the $K^{\mp}\pi^{\pm}$ mass combinations fulfilling $|m(K^{\mp}\pi^{\pm}) - m_{D^0}| < 70$ MeV. The solid line represents the result of the fit described in the text. The shaded histogram shows the background expectation from the like sign $K^{\pm}\pi^{\pm}$ pairs.

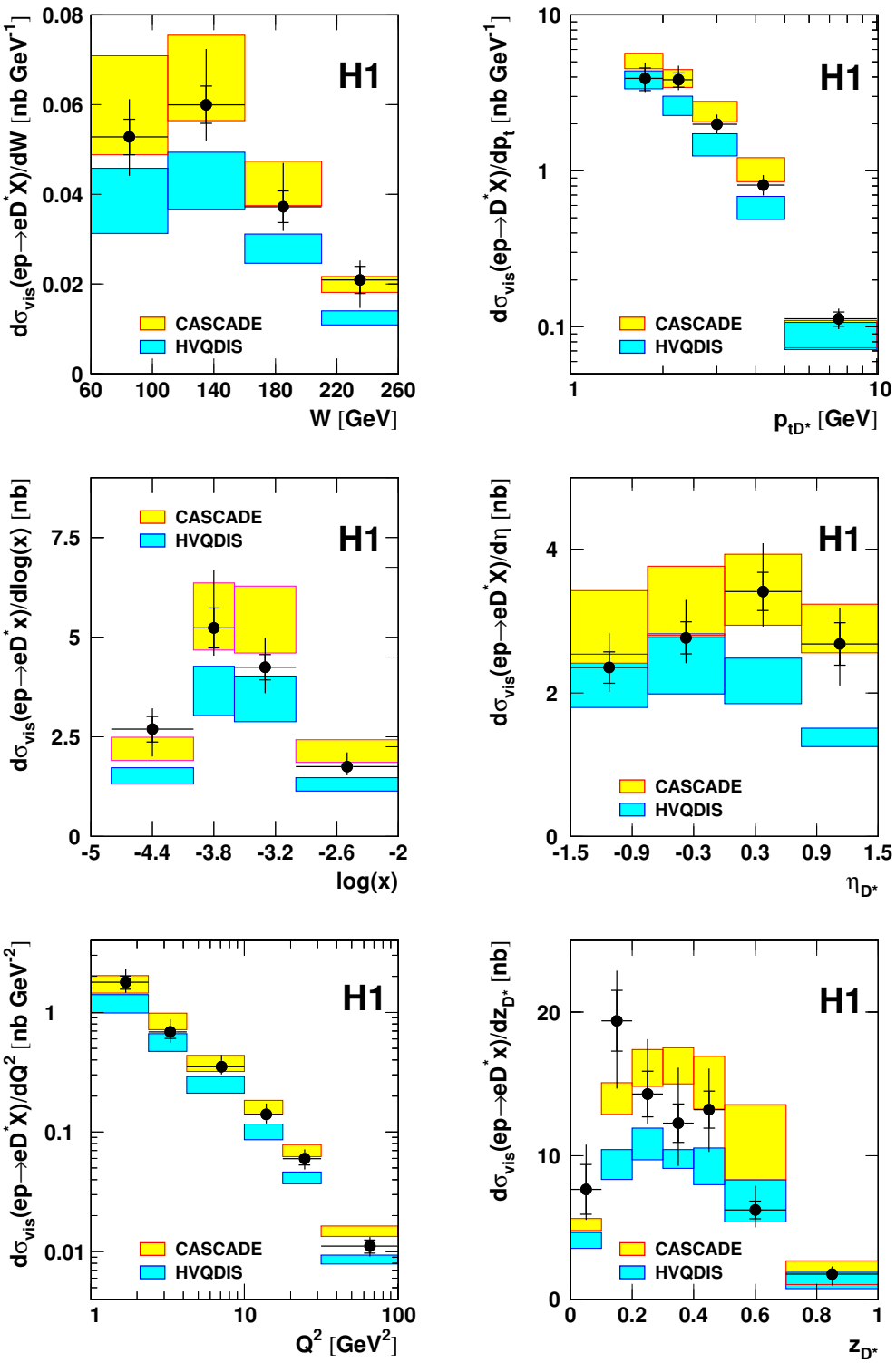


Figure 2: Single differential inclusive cross section $\sigma(ep \to eD^{*\pm}X)$ versus $W$, $x$, $Q^2$ and $p_{t\,D^*}$, $\eta_{D^*}$, $z_{D^*}$. The inner and outer error bars correspond to the statistical and the total errors. The expectation of the NLO DGLAP calculation using HVQDIS with GRV98-HO parton densities is indicated by the lower shaded band. The upper shaded band is the expectation of the CCFM calculations based on the CASCADE program with the initial gluon distribution fitted to the inclusive $F_2$ data. The upper and lower bounds of both calculations correspond to ($m_c = 1.3$ GeV, $\epsilon_c = 0.035$) and ($m_c = 1.5$ GeV, $\epsilon_c = 0.10$), respectively.

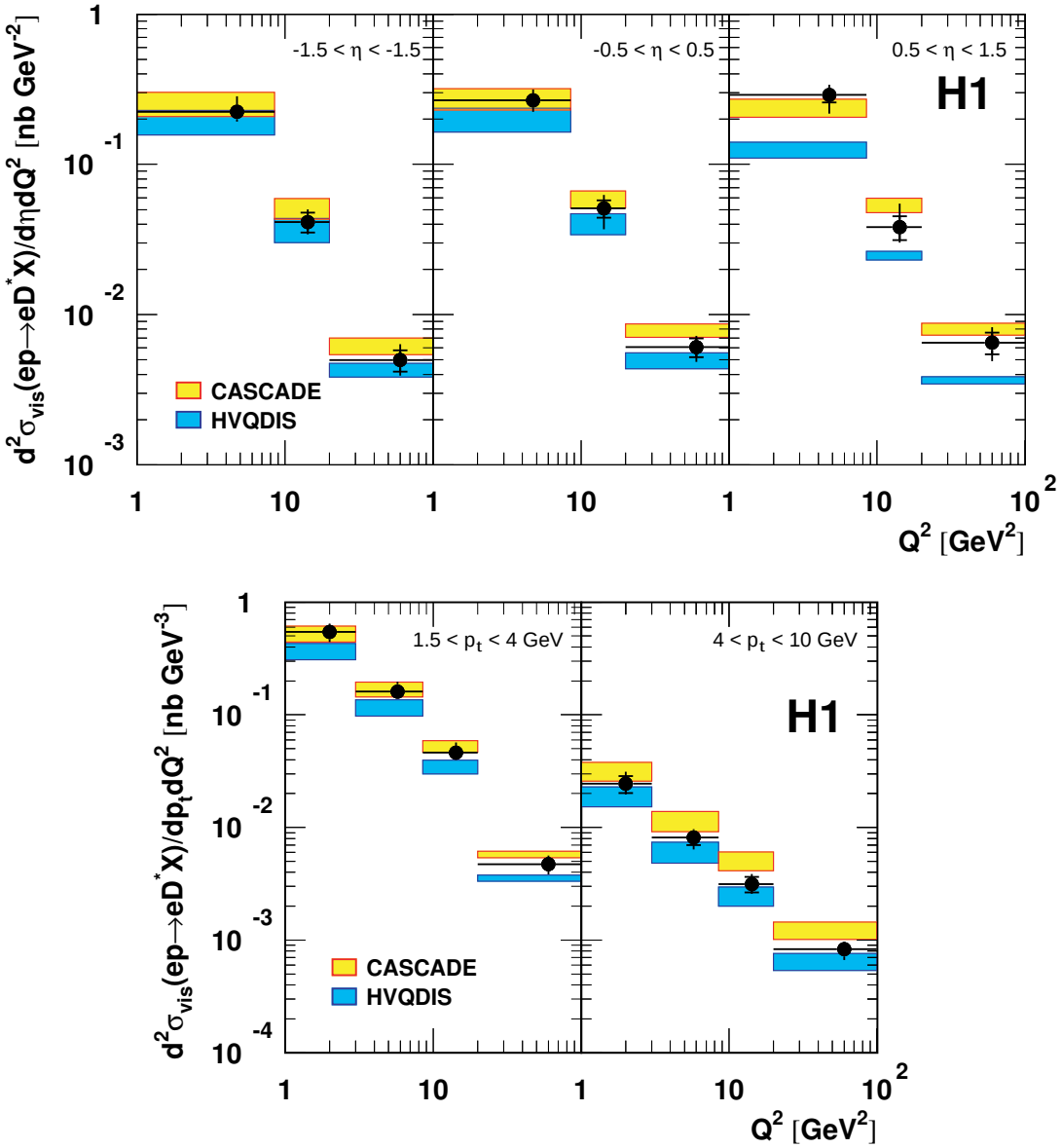


Figure 3: Double differential inclusive cross section $\mathrm{d}^2\sigma/\mathrm{d}\eta\mathrm{d}Q^2$ and $\mathrm{d}^2\sigma/\mathrm{d}p_t\mathrm{d}Q^2$ in bins of $\eta_{D^*}$ and $p_{t\,D^*}$ (see figure 2 for details).

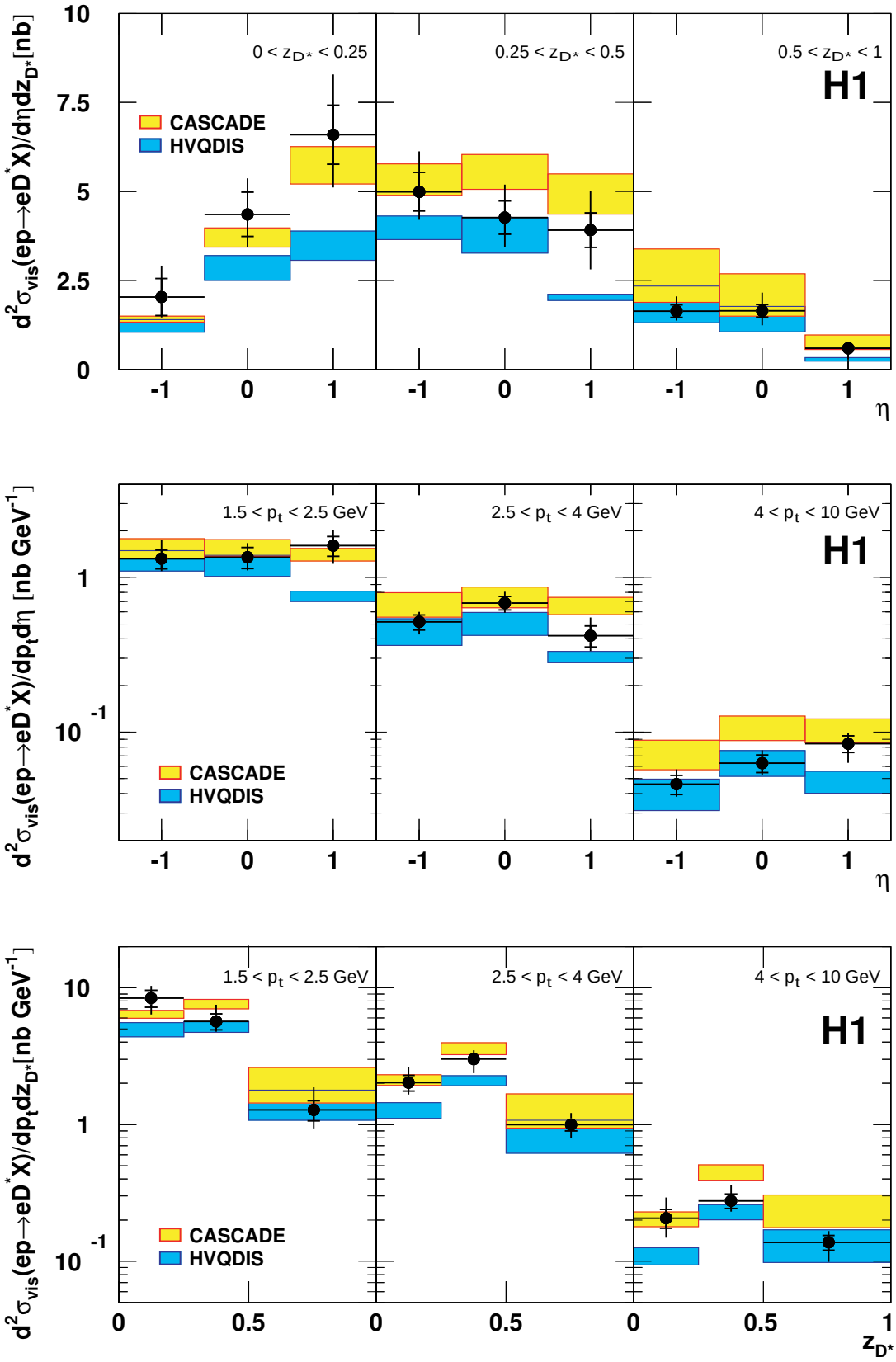


Figure 4: Double differential inclusive cross section $\mathrm{d}^2\sigma/\mathrm{d}\eta\mathrm{d}z_{D^*}$ in bins of $z_{D^*}$ and $\mathrm{d}^2\sigma/\mathrm{d}p_t\mathrm{d}z_{D^*}$ and $\mathrm{d}^2\sigma/\mathrm{d}p_t\mathrm{d}\eta$ in bins of $p_{t\,D^*}$ (see figure 2 for details).

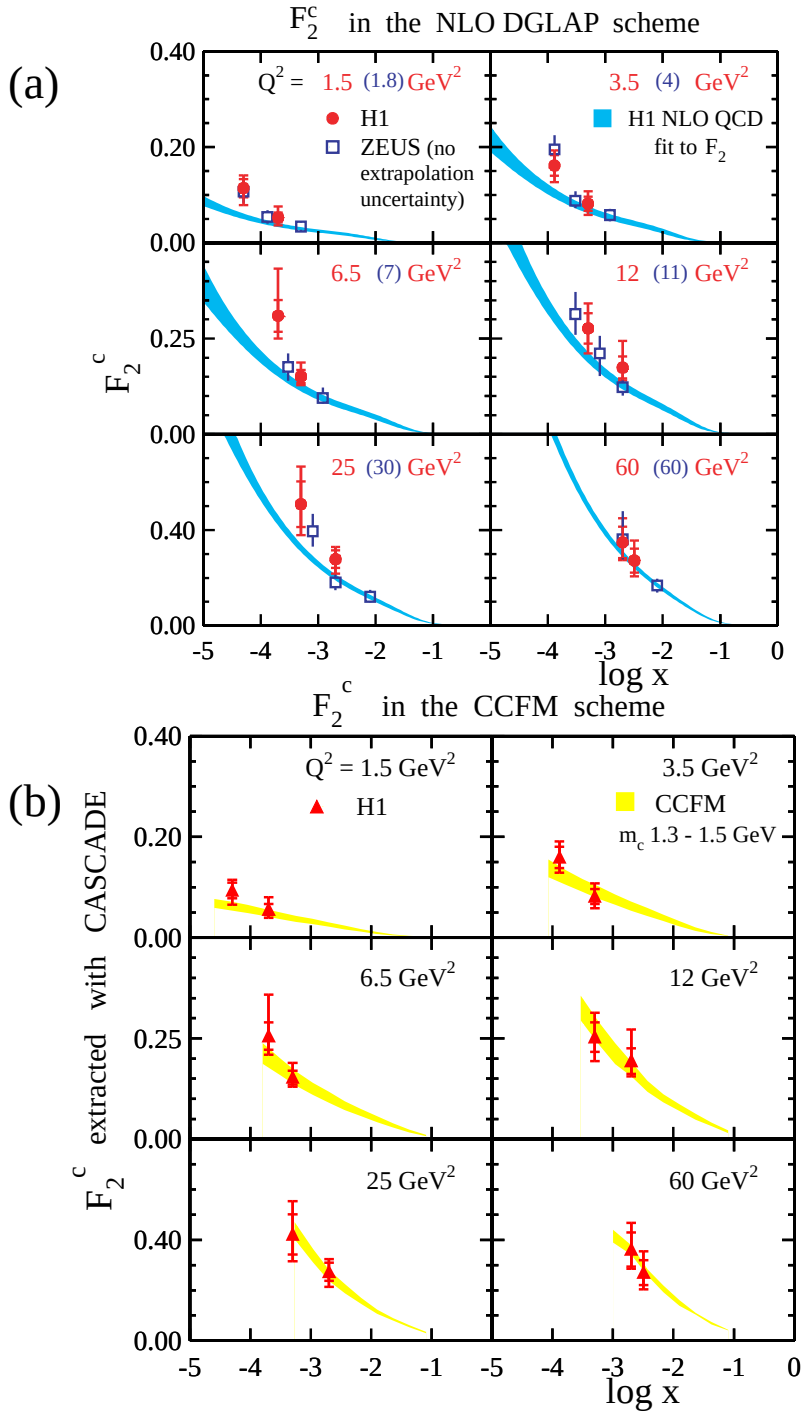


Figure 5: $F_2^c$, as derived from the inclusive $D^{*\pm}$ meson analysis (a) in the framework of NLO DGLAP and (b) in the framework of CCFM, both for $m_c = 1.4$ GeV. The error bars on the H1 data points refer to the statistical (inner) and the total (outer) error, respectively. In (a) the shaded bands represent the predictions of $F_2^c$ from the H1 NLO DGLAP fit to the inclusive $F_2$ measurements including all the uncertainties described in the text. The dominant contribution arises from the uncertainty of $m_c$. The ZEUS measurements [3] are shown for comparable values of $Q^2$ indicated in parantheses (see [3] for a discussion of the extrapolation uncertainties). In (b) the bands represent the expectation of $F_2^c$ from the fit to the inclusive $F_2$ in the CCFM scheme including only the variation of $m_c$ which in both cases ranges from $1.3$ to $1.5$ GeV.

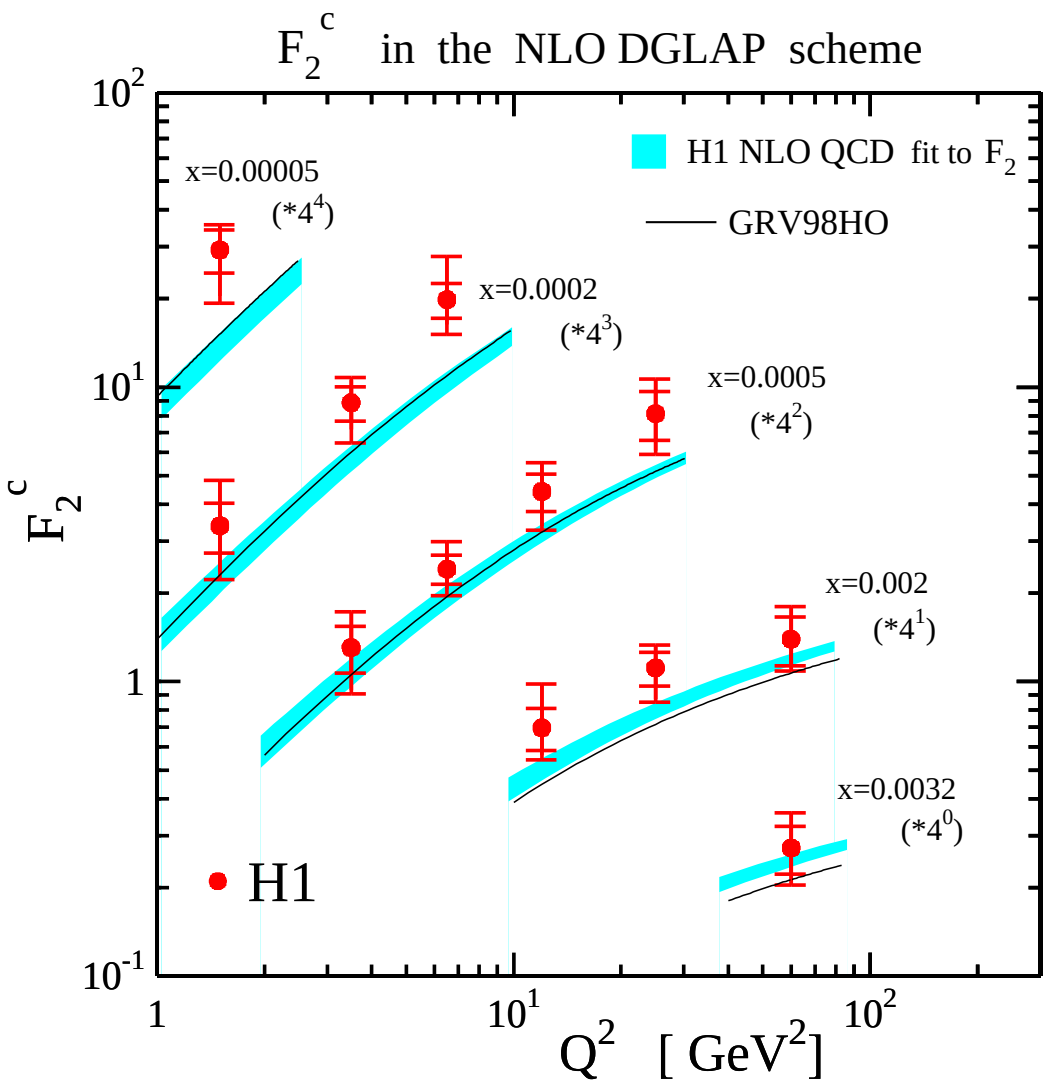


Figure 6: $F_2^c$ as derived from the inclusive $D^{*\pm}$ meson production cross section as a function of $Q^2$ for different values of $x$. The error bars refer to the statistical (inner) and the total (outer) error, respectively. The shaded bands represent the predictions of the NLO DGLAP evolution based on the parton densities in the proton obtained by the fit to the inclusive $F_2$ for $m_c = 1.4$ GeV including all uncertainties described in the text. The black lines show the predictions in the NLO DGLAP scheme for $m_c = 1.4$ GeV using the gluon density from GRV98-HO.

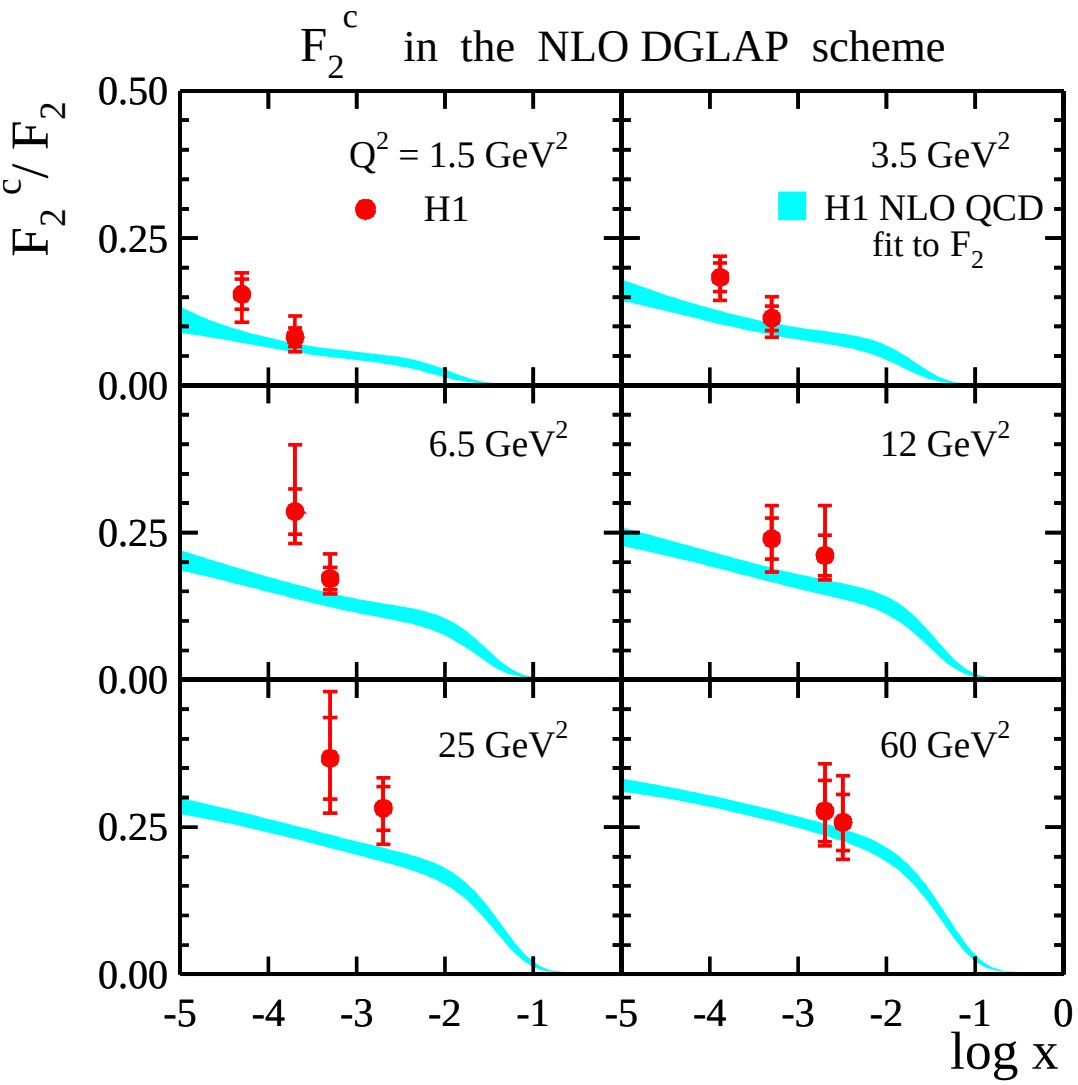


Figure 7: The ratio of $F_2^c$ over $F_2$ as derived from the inclusive $D^{*\pm}$ meson analysis as a function of $x$ for different values of $Q^2$. The error bars refer to the statistical (inner) and the total (outer) error, respectively. The shaded bands represent the predictions of the NLO DGLAP evolution based on the parton densities in the proton obtained by the fit to the inclusive $F_2$ for a central charm quark mass of $1.4$ GeV including all uncertainties.